

Process characterization with Monte Carlo wave functions

J. Gulliksen, D. D. Bhaktavatsala Rao, and K. Mølmer

Department of Physics and Astronomy, Aarhus University, Ny Munkegade 120, DK-8000 Aarhus C, Denmark

(Received 20 September 2013; published 26 November 2013)

We present an efficient method to simulate a quantum process subject to dissipation and noise. To describe the effect on any input state we evolve Monte Carlo wave functions for a principal and ancilla system, prepared initially in an entangled state. In analogy to experimental process tomography, the simulated propagator for the system density matrix is conveniently described by a process χ matrix - directly determined from the stochastic state vectors. Our method significantly reduces the computational complexity compared with standard theoretical characterization methods. It also delivers an upper bound on the trace distance between the ideal and simulated process based on the evolution of only a single wave function of the entangled system.

DOI: [10.1103/PhysRevA.88.052129](https://doi.org/10.1103/PhysRevA.88.052129)

PACS number(s): 03.65.Wj, 32.80.Qk, 42.50.Dv

I. INTRODUCTION

Characterization of quantum-dynamical systems is a prerequisite for high-fidelity quantum computing and information protocols. Two tools created for this purpose are quantum-state and quantum-process tomography. Quantum-state tomography takes the measurement data of a quantum system's unknown state and identifies the representative density operator ρ . Quantum-process tomography is concerned with experimentally characterizing a process \mathcal{E} so that the output state may be predicted from any given input state, $\rho \rightarrow \mathcal{E}(\rho)$.

To completely characterize an N -qubit process, standard quantum process tomography (SQPT) [1–3] requires implementation on a number of input states that scales exponentially with the number of qubits. Avoiding the preparation of many different input states ancilla-assisted quantum process tomography (AAPT) [4–7] was proposed as an alternative. Here the information of all input states is encoded into a single maximally entangled system-ancilla state in a doubled Hilbert space. While both SQPT and AAPT rely on state tomography of the output state, direct characterization of quantum dynamics [8,9] addresses features of the underlying dynamics via suitable “probe” systems and corresponding measurements. For more details and an investigation of resource demands for each of these strategies see Ref. [10].

If a quantum system is subject to unitary and dissipative dynamics, it is a nontrivial task to theoretically determine the resulting process \mathcal{E} from a general input state to its corresponding output state. Solving that problem is highly relevant in quantum information science, as it quantifies not only the fidelity of gates for different input states but also the dominant error mechanisms. This may in turn eventually point to improved gates by appropriate control schemes. In this paper we distinguish between (experimental) process tomography and (theoretical) characterization of a process by solution of the master equation. A theoretical χ matrix may be compared with experiments to validate interaction parameters [11,12]. It may also be applied to investigate how errors accumulate when processes are applied to states, which are themselves the outcome of previous interactions, e.g., in a quantum computer algorithm.

This article will present a procedure to numerically determine the quantum process \mathcal{E} from the master equation

governing time-dependent system dynamics. Monte Carlo wave functions [13–16] have allowed a numerically efficient alternative to the ordinary master equation approach to obtain the time-dependent density matrix $\rho(t)$. Indeed, a Monte Carlo simulation of a quantum system with a Hilbert space of size D ($D \gg 1$) involves far fewer variables ($\sim D$) than its master equation counterpart ($\sim D^2$). In this paper we simulate the evolution of our system from an initial maximally entangled state with a nonevolving ancilla system, and we show that the Monte Carlo wave functions for this combined system can be directly processed to yield information about the quantum process \mathcal{E} .

The paper is organized as follows. In Sec. II we introduce the system master equation as well as the general problem of characterizing the time evolution as a quantum process applied to any initial state. In Sec. III we introduce part of the formalism needed for process characterization and describe density matrix schemes that yield the process matrix χ . In Sec. IV we briefly recall the Monte Carlo wave function method and relevant aspects of its implementation in this work. In Sec. V we show how the time-evolved Monte Carlo wave functions can be used to yield stochastic “process vectors” ζ that directly average to the process matrix χ . In Sec. VI we show how the no-jump, single wave function trajectory yields a readily accessible upper bound on the trace distance between the actual process matrix and any desired process matrix, a useful measure of process fidelity. In Sec. VII we apply our method to the simulation of a Rydberg blockade C-PHASE gate, subject to realistic decay and dephasing mechanisms. Section VIII concludes the paper.

II. CHARACTERIZING OPEN QUANTUM SYSTEMS

The simulation of dissipative quantum systems is important to quantum information processing as it allows realistic modeling of quantum gate protocols. Because of dissipation, the time-evolution is not unitary and the dynamics must be treated using a master-equation approach. This linear equation, describing time evolution of the principal system's density matrix ρ , is typically obtained by making use of the Born-Markov approximations and tracing a larger composite density matrix over the reservoir degrees of freedom associated with the dissipation processes. Denoting the Hamiltonian for the

principal system by H , the master equation may be written as

$$\dot{\rho} = -\frac{i}{\hbar}[H, \rho] + \mathcal{L}_{\text{relax}}(\rho), \quad (1)$$

where we consider the relaxation operator $\mathcal{L}_{\text{relax}}$ in Lindblad form [17]:

$$\mathcal{L}_{\text{relax}}(\rho) = -\frac{1}{2} \sum_k (L_k^\dagger L_k \rho + \rho L_k^\dagger L_k) + \sum_k L_k \rho L_k^\dagger. \quad (2)$$

Equation (1) preserves the positivity and normalization of the density operator ρ , and the L_k operators in Eq. (2) act in the space of the principal system. Thus by solving Eq. (1) with the, possibly time-dependent, Hamiltonian corresponding to a complex quantum gate operation we determine the evolution of any initial state under the influence of damping and noise. This evolution from $t = 0$ to $t = \tau$ can be written as a linear transformation of the input density matrix elements, $\rho_{ij}(\tau) = \sum_{mn} M_{ij,mn} \rho_{mn}(0)$.

As a guarantee for trace preservation and positivity the solution for the density matrix $\rho(\tau) = \mathcal{E}(\rho(0))$ may also be described in the operator-sum representation [18]

$$\mathcal{E}(\rho) = \sum_i K_i \rho K_i^\dagger, \quad (3)$$

where the Kraus operators K_i act on the system's Hilbert space and obey $\sum_i K_i^\dagger K_i = 1$. Picking the Hermitian operators $\{E_m\}$ as a basis for the set of all operators on the principal system's Hilbert space¹ we may write any quantum process as

$$\mathcal{E}(\rho) = \sum_{mn} \chi_{mn} E_m \rho E_n^\dagger. \quad (4)$$

The characterization matrix χ_{mn} in Eq. (4) is related to the Kraus form (3) via the expansion of each $K_i = \sum_m e_{im} E_m$, and the identification $\chi_{mn} = \sum_i e_{im} e_{in}^*$.

Suppose a process is simulated with the master equation, for which the accumulated effect of the unitary and dissipative dynamics on the quantum system is not known *a priori*. From the simulation data, we want an efficient method to obtain the full information about \mathcal{E} . In the next section standard methods of acquiring χ_{mn} , and thus \mathcal{E} , will be shown.

III. PROCESS CHARACTERIZATION SCHEMES

In the following discussion we consider a general quantum system with Hilbert space dimension D . Assuming the map \mathcal{E} is trace preserving, then characterization of \mathcal{E} is equivalent to a determination of the $D^4 - D^2$ independent elements of χ [1].

Let $\mathcal{O}_{pq} = |p\rangle\langle q|$ for $p, q \in \{1, \dots, D\}$ be a linearly independent basis for the space of $D \times D$ linear operators. Cataloging the action of the fixed operator basis $\{E_m\}$ on all input matrices we create the $D^4 \times D^4$ matrix \mathcal{K} :

$$E_m \mathcal{O}_{rs} E_n^\dagger = \sum_{pq} \mathcal{K}_{rs,pq}^{mn} \mathcal{O}_{pq}. \quad (5)$$

¹In a multiqubit system, an appropriate operator basis might be tensor products of the identity and Pauli operators for each qubit.

A. Standard quantum process characterization

In standard quantum process characterization (SQPC) the effect of the process \mathcal{E} is determined: Experimentally, D^2 different input states (density matrices) are subjected to the physical process and the resulting output states are measured by quantum state tomography. In a theoretical analysis, the master equation is used to simulate the process, and the outcome solution $\mathcal{E}(\mathcal{O}_{rs})$ for input matrices \mathcal{O}_{pq} is expressed as a linear combination in the same operator basis:

$$\mathcal{E}(\mathcal{O}_{rs}) = \sum_{pq} \Lambda_{rs,pq} \mathcal{O}_{pq}. \quad (6)$$

Combining Eqs. (4)–(6) we obtain $\sum_{mn} \mathcal{K}_{rs,pq}^{mn} \chi_{mn} = \Lambda_{rs,pq}$, which in matrix form reads

$$\mathcal{K} \chi = \Lambda. \quad (7)$$

Finding $\{\chi_{mn}\}$ from the simulated $\{\Lambda_{rs,pq}\}$ is now a linear algebra problem, although in general it is not uniquely determined by Eq. (7).

Let us here make an estimate of how the computational resources needed to perform SQPC scales with Hilbert space dimension. Simulating a process with the master equation requires solving D^2 coupled differential equations for each of the D^2 input states; that is, we must solve D^4 differential equations. Solution of Eq. (7) requires decomposition of \mathcal{K} , using the Cholesky method for example, followed by forward and back substitution for χ . The computational complexity of a straightforward decomposition is $O(D^{12})$ while the substitution operations are each $O(D^8)$.

For applications to quantum computing on a register composed of N L -level quantum systems, the product Hilbert space has the dimension $D = L^N$. If the operators E_m are taken to be $SU(L)$ operator products, the product nature simplifies decomposition of \mathcal{K} into separate $O(L^{12})$ problems.

B. Ancilla-assisted process characterization

In ancilla-assisted process characterization (AAPC), instead of composing Λ by propagating separate, initial matrices \mathcal{O}_{rs} , all input states are simultaneously represented in a “super” operator

$$\mathcal{O} = \sum_{rs} \mathcal{O}_{rs} \otimes \mathcal{O}_{rs} \quad (8)$$

on the combined principal (P) and ancilla (A) system. This expanded system is now made subject to the quantum process, $\mathcal{E}_{P \otimes A}(\mathcal{O}) \rightarrow \mathcal{O}_{\text{out}}$, which acts with the original process \mathcal{E} only on the principal system component:

$$\mathcal{O}_{\text{out}} \equiv (\mathcal{E} \otimes \mathcal{I})(\mathcal{O}). \quad (9)$$

The identity operator \mathcal{I} in Eq. (9) acts on the ancilla's operator space. From Eq. (8) we have $(\mathcal{E} \otimes \mathcal{I})(\mathcal{O}) = \sum_{rs} \mathcal{E}(\mathcal{O}_{rs}) \otimes \mathcal{O}_{rs}$, implying that a single master equation simulation on the expanded system allows calculation of all $\mathcal{E}(\mathcal{O}_{rs})$. The ancilla system is used to extract separate results,

$$\mathcal{E}(\mathcal{O}_{rs}) = \text{Tr}_A[(I \otimes |s\rangle\langle r|) \mathcal{E}_{P \otimes A}(\mathcal{O})], \quad (10)$$

where Tr_A denotes partial trace on the ancilla's Hilbert space. Then in a way equivalent to Eq. (6) we may expand $\mathcal{E}(\mathcal{O}_{rs})$

into the basis of $\{\mathcal{O}_{pq}\}$ and retrieve the characterization matrix χ from Eq. (7).

Simulating a quantum process with AAPC involves solving D^4 differential equations for the expanded input state. The complexity of solving Eq. (7) remains $O(D^{12})$ and $O(D^8)$ for decomposition of \mathcal{K} and forward and backward substitution, respectively.

IV. MONTE CARLO WAVE FUNCTIONS

We can obtain the predictions made by the master equation (1) by introducing a stochastic element into the evolution of so-called Monte Carlo wave functions [14–16]. These are wave functions $|\psi(t)\rangle$ propagated with the non-Hermitian Hamiltonian $H_{\text{eff}} = H - i\hbar/2 \sum_k L_k^\dagger L_k$. Due to the nonunitary evolution during a small time step dt ,

$$|\psi_0(t+dt)\rangle = \left(1 + \frac{1}{i\hbar} H_{\text{eff}} dt\right) |\psi(t)\rangle, \quad (11)$$

the square of the norm associated with $|\psi_0(t+dt)\rangle$ is reduced by

$$\delta p = \sum_k \delta p_k = dt \sum_k \langle \psi(t) | L_k^\dagger L_k | \psi(t) \rangle. \quad (12)$$

The next step involves a random choice. Either the wave function $|\psi_0(t+dt)\rangle$ is renormalized, or, with probability δp , the wave function is subject to a quantum jump. This constitutes a collapse of the wave function, and with a branching ratio of $\delta p_k/\delta p$, the final state is chosen among the states $L_k|\psi(t)\rangle$. Thus, at time $t+dt$ we have one of the following possibilities:

$$\text{with prob. } 1 - \delta p, \quad |\psi(t+dt)\rangle = \frac{|\psi_0(t+dt)\rangle}{\sqrt{1 - \delta p}}, \quad (13a)$$

$$\text{with prob. } \delta p_k, \quad |\psi(t+dt)\rangle = \frac{L_k |\psi(t)\rangle}{\sqrt{\delta p_k/dt}}. \quad (13b)$$

An ensemble of wave functions subject to this dynamics will on average reproduce the time-dependent solution of the master equation.

The validity of the calculation relies on time steps much smaller than the time scale of the coherent and incoherent physical processes. However, the direct implementation discussed above may be reformulated [16,19] such that quantum jumps are not decided in terms of expression (12), linear in the “small” time step dt . Instead, the “no-jump” wave function $|\psi_0(t)\rangle$ is allowed to evolve until its norm reaches a predetermined random number uniformly distributed between 0 and 1. At this time a jump is made in the manner of Eq. (13b). In this way integration of Eq. (11) can be left to an accurate and efficient numerical solver. In our implementation to a physical example below, we use a variant of the Adams-Bashford method which utilizes adaptive step-size control.

V. PROCESS CHARACTERIZATION WITH MONTE CARLO

Since density matrices in the master equation approach are replaced by state vectors, simulation by Monte Carlo wave

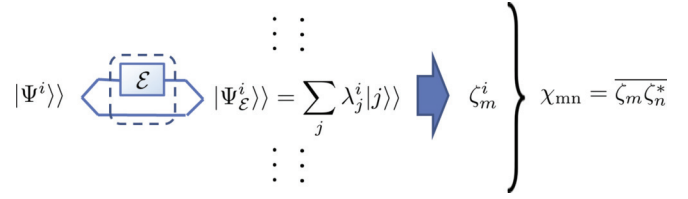


FIG. 1. (Color online) Implementation of AAPC with Monte Carlo wave functions: In each trajectory i , the evolution of the entangled system and ancilla is simulated, subject to the process $\mathcal{E} \otimes I$. From the expansion coefficients λ_j , we determine the vector of components ζ_m . Averaging over many simulation outcomes $\zeta_m^i \zeta_n^{i*}$ the χ matrix is obtained.

functions allows access to larger quantum systems. How this benefits process characterization is the focus of this section. We first analyze ancilla-assisted process characterization using Monte Carlo wave functions (AAWF) and discuss its advantages over standard characterization techniques. We conclude the section with a discussion of why the ancilla strategy is preferred over a Monte Carlo treatment of standard quantum process tomography.

Observe that the super operator in Eq. (8) is a pure state projection operator, that is, $\mathcal{O} = |\Psi\rangle\langle\Psi|$, where the bipartite wave function $|\Psi\rangle = \sum_r |r\rangle \otimes |r\rangle$ describes the principal system maximally entangled with an identical ancilla system. Evolution of \mathcal{O} is then equivalent to propagation of $|\Psi\rangle \rightarrow |\Psi_\mathcal{E}\rangle$ under the rules of Monte Carlo wave functions; that is, averaging the outer product of the resulting states over many simulated outcomes we find $|\Psi_\mathcal{E}\rangle\langle\Psi_\mathcal{E}| = (\mathcal{E} \otimes \mathcal{I})(\mathcal{O})$.

Next we construct κ , the “wave function” analog of standard tomography’s \mathcal{K} matrix. This is a $D^2 \times D^2$ matrix matrix of expansion coefficients for the application of the standard operators $\{E_m\}$ of Sec. II,

$$(E_m \otimes I)|\Psi\rangle = \sum_j \kappa_j^m |j\rangle, \quad (14)$$

where $\{|j\rangle : j = 1, \dots, D^2\}$ is a linearly independent basis for the D^2 -dimensional vectors on the principal-ancilla space $P \otimes A$.

For each simulated Monte Carlo wave function $|\Psi_\mathcal{E}\rangle = \sum_j \lambda_j |j\rangle$ we now define the ζ vector as the solution to

$$\sum_m \kappa_j^m \zeta_m = \lambda_j. \quad (15)$$

The coefficients λ_j , and hence ζ_m , carry information about the process \mathcal{E} . Indeed, when averaging the ζ vector coordinates over a sufficiently large ensemble of Monte Carlo wave functions we directly obtain the process matrix of Eq. (4),

$$\chi_{mn} = \overline{\zeta_m \zeta_n^*} \quad (16)$$

(see Appendix).

The implementation of the AAWF method is illustrated in Fig. 1. To propagate $|\Psi\rangle$ in a single Monte Carlo trajectory we must solve $D \times D$ coupled differential equations. Thus, averaging over n trajectories requires solving $nD \times D$ coupled differential equations, which may be much less than the D^4 equations needed by standard techniques. Even more striking

TABLE I. Numerical cost of characterizing a quantum process on a D -dimensional Hilbert space. The first column lists the density matrix and Monte Carlo approaches to standard (SQPC) and ancilla-assisted (AAPC) process characterization. The second column (c.d.e.) lists the number of coupled differential equations needed to simulate the time evolution. The last column (s.l.e.) lists the cost of solving the system of linear equations for the χ matrix/ ζ vector, assuming a Cholesky decomposition of the matrix \mathcal{K} (κ).

Technique	c.d.e.	s.l.e.
SQPC		
Density matrix	$D^2 \times D^2$	$O(D^8)$
Monte Carlo	$nD^2 \times D$	$O(D^8)$
AAPC		
Density matrix	$D^2 \times D^2$	$O(D^8)$
Monte Carlo	$nD \times D$	$n \times O(D^4)$

is the reduction in cost associated with the decomposition of κ , which scales as a $O(D^6)$ problem, compared to the $O(D^{12})$ problem of decomposing the \mathcal{K} matrix. Each of the n Monte Carlo simulations at output creates a size $O(D^4)$ problem when using forward or backward substitution to solve for the ζ vector.

Analogous to standard process characterization, we might have used Monte Carlo wave functions to simulate input states in the original Hilbert space, construct the output density matrices, and subsequently solve for χ . However, implementation requires simulating n size D Monte Carlo wave functions for all D^2 input states, which is a larger problem than its AAPC counterpart (Table I). Also, this method does not allow for a ζ vector equivalent, meaning no reduction in the complexity of solving Eq. (7).

Note that the decomposition of \mathcal{K} concerns only structural properties of the chosen operator and state bases of the quantum system and is independent of the physical process \mathcal{E} . The same is true for the vector variant, applied to the analysis of Monte Carlo wave functions. Indeed, our vector formulation of the problem shows that the simpler decomposition of κ offers an effective reduction of the costs to decompose \mathcal{K} , which is applicable for standard process characterization.

VI. AN UPPER BOUND ERROR ESTIMATE FROM A SINGLE WAVE FUNCTION

A meaningful measure between the ideal ($\tilde{\chi}$) and the actual (χ) process matrices in a physical gate operation is the trace distance [20]. The trace distance is a translationally invariant metric on the space of Hermitian, positive semidefinite matrices of unit trace, and it is given by $T(\tilde{\chi}, \chi) \equiv \frac{1}{2} \|\tilde{\chi} - \chi\|_{tr}$, where $\|A\|_{tr} = \text{Tr}(\sqrt{A^\dagger A})$ is the trace norm.

We are interested in the characterization of the effect of noise and dissipation on gate operations in quantum computing. To have any relevance for quantum computation such gates may experience only weak noise. This implies that in the majority of Monte Carlo simulations, the wave functions should follow the “no-jump” trajectory (13a) through the entire duration of the process. With the AAWF method, the calculation of this single wave function provides a useful indication of the gate’s performance.

The simulated Monte Carlo wave functions making up a AAWF calculation of χ may be separated into two parts: those that never jumped, yielding a single ζ vector and corresponding χ matrix, $\chi_S = \zeta_S \zeta_S^\dagger$, and those that jumped at randomly assigned times to yield a set of vectors ($\chi_i = \zeta_i \zeta_i^\dagger$). The fraction $\frac{S}{n}$ of no-jump wave functions is equal to the product of the normalization factors $(1 - \delta p)$ in Eq. (13a) applied over time. The remaining fraction $\frac{J}{n}$ of the simulated ensemble ($n = J + S$ being the total number of trajectories) yields the sum of terms $\chi_J = \frac{1}{J} \sum_{i=1}^J \zeta_i \zeta_i^\dagger$. Finally we see that

$$\chi = \frac{S}{n} \chi_S + \frac{J}{n} \chi_J. \quad (17)$$

Calculating the trace distance between Eq. (17) and the ideal process matrix $\tilde{\chi}$ we employ the triangle inequality and translational invariance to obtain

$$T\left(\tilde{\chi}, \frac{S}{n} \chi_S + \frac{J}{n} \chi_J\right) \leq T\left(\tilde{\chi} - \frac{S}{n} \chi_S, 0\right) + T\left(0, \frac{J}{n} \chi_J\right). \quad (18)$$

Since $T(0, \frac{J}{n} \chi_J) = \frac{1}{2} \|\frac{J}{n} \chi_J\|_{tr} = \frac{J}{2n}$, this provides an upper bound on the trace distance using the evolution of only a single no-jump wave functions and its associated χ matrix:

$$T(\tilde{\chi}, \chi_S + \chi_J) \leq T\left(\tilde{\chi}, \frac{S}{n} \chi_S\right) + \frac{J}{2n}. \quad (19)$$

Clearly this upper bound is of limited value if dissipation is significant and many wave functions jump.

Another typical measure for the effect of error in a process is fidelity $F(\tilde{\chi}, \chi) \equiv \|\sqrt{\tilde{\chi}} \sqrt{\chi}\|_{tr}$. However, being a nonlinear expression it has a more complicated relation with the different components of the wave function ensemble. We shall return to both process error measures in the numerical example below.

VII. C-PHASE GATE

As an example of our process characterization, we consider the controlled-phase (C-PHASE) gate operation between atoms coupled by the Rydberg blockade interaction (Fig. 2). Each atom has four levels: two ground levels which comprise the qubit space, the Rydberg level with which the atoms interact, and the intermediate level which facilitates transitions to the Rydberg level via a two-photon process. Thus, even though the initial state space and resulting process matrix may be restricted to the qubit space, we are still required to simulate the system considering all levels. Obtaining the χ matrix even for the simplest two-qubit gates is nontrivial, and extending it beyond two atoms becomes computationally challenging for standard characterization strategies. Meanwhile, the proposed AAWF method can readily deal with multiqubit process characterization involving up to 8–10 atoms.

A C-PHASE gate on the $5s_{1/2}$ hyperfine states $|0\rangle \equiv |F=1, m_F=0\rangle$ and $|1\rangle \equiv |F=2, m_F=0\rangle$ involves single-qubit rotations between $|1\rangle$ and the Rydberg state $|r\rangle = |97d_{5/2}, m_j=5/2\rangle$. This is a two-photon process, achieved with σ_+ polarized 780 and 480 nm beams. The 780 nm beam is tuned by an amount Δ to the red of the $|1\rangle \rightarrow |p\rangle \equiv |5p_{3/2}, F=3\rangle$ transition while the 480 nm beam is also tuned an amount Δ to the blue of the $|p\rangle \rightarrow |r\rangle$ transition. The

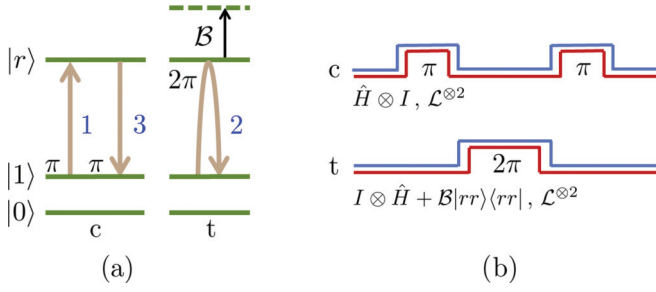


FIG. 2. (Color online) Rydberg-mediated controlled phase gate. (a) Illustration of (1) a resonant transfer between $|1\rangle$ and $|r\rangle$ of the control atom c , (2) subsequent coherent excitation and de-excitation between $|1\rangle$ and $|r\rangle$ of the target atom t , yielding the controlled phase shift on the $|1\rangle$ component, unless the control atom is excited and providing the Blockade shift \mathcal{B} , and (3) de-excitation of the control atom. (b) Illustration of the pulse sequence and listing the Hamiltonian and driving terms. The identity operator I signifies individual addressing of atoms, $\mathcal{L}^{\otimes 2} = -\frac{i\hbar}{2}(\sum_m L_m^\dagger L_m \otimes I + I \otimes \sum_m L_m^\dagger L_m)$ describes decoherence in the system, and the two-atom interaction $\mathcal{B}|rr\rangle\langle rr|$ prevents both atoms from occupying the Rydberg state. The single-qubit Hamiltonian \hat{H} is discussed in detail in the text.

resulting Rabi frequencies are Ω_R (Ω_B) for the red (blue) detuned laser. After adiabatically eliminating $|p\rangle$ from the Hamiltonian describing this process for numerical efficiency, we find in the rotating-wave approximation [21]:

$$\hat{H} = \underbrace{\frac{(2\Delta - \delta E_r)\Omega_R\Omega_B}{8\Delta(\Delta - \delta E_r) + 2\gamma^2}}_{\Omega_{\text{eff}}/2} |1\rangle\langle r| + \text{H.c.} + \left(\delta E_0 - \frac{\Delta\Omega_R^2}{4\Delta^2 + \gamma^2} \right) |0\rangle\langle 0|. \quad (20)$$

Here

$$\delta E_r \simeq \frac{16\Delta^2(\Omega_B^2 - \Omega_R^2) - \Omega_R^4}{64\Delta^3} \quad (21)$$

is subtracted from the “blue” detuning to compensate for suboptimal Rabi-oscillations due to Stark shifts arising from power differences between the red and blue detuned lasers. Similarly, δE_0 may be used to balance the $|0\rangle\langle 0|$ term, ensuring no phase contributions from $|0\rangle$ caused by the red laser. Finally, γ is the decay rate from $|p\rangle$.

The effective operator formalism [21] provides us with a mechanism to simulate decay from $|p\rangle$, *viz.*,

$$\hat{L}_{\gamma_p, j} = \frac{\sqrt{c_j\gamma_p}\Omega_R}{2\Delta - i\gamma} |j\rangle\langle 1| + \frac{\sqrt{c_j\gamma_p}\Omega_B}{2(\Delta - \delta E_r) - i\gamma} |j\rangle\langle r|, \quad (22)$$

where $j \in \{0, 1, g\}$ and c_j are the branching ratios $\{0.12, 0.32, 0.56\}$ for decay from $|p\rangle$, that is, $\gamma = \sum_j c_j\gamma_p$. It is appropriate here to discuss $\hat{L}_{\gamma_p, g}$ because $|g\rangle$ does not feature in the system Hamiltonian. Decay events into the “loss state” $|g\rangle$ do not couple back into the system, and a Monte Carlo trajectory is merely disposed when a jump of this sort is simulated.

Magnetic field noise and atomic motion are important dephasing sources that we describe in Monte Carlo simulation by the jump operator [15]

$$\hat{L}_{\gamma_d} = \sqrt{\gamma_d}(\mathbb{1} - 2|r\rangle\langle r|), \quad (23)$$

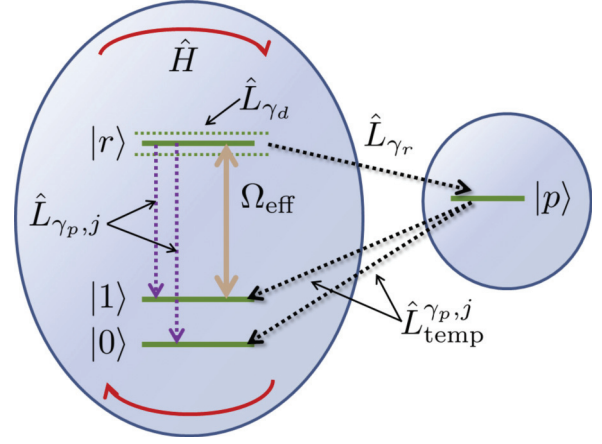


FIG. 3. (Color online) For numerical efficiency the short-lived, intermediate state $|p\rangle$ is adiabatically eliminated and yields an effective description with couplings (Ω_{eff}) and dissipation terms ($\hat{L}_{\gamma_d}, \hat{L}_{\gamma_p, j}$) shown in the left part of the figure. For convenience, $|p\rangle$ is formally reintroduced to represent decay events from $|r\rangle$ (see text).

where $\mathbb{1}$ is shorthand for the identity operator. Spontaneous emission from $|r\rangle$, described by the jump operator

$$\hat{L}_{\gamma_r} = \sqrt{\gamma_r}|p\rangle\langle r|, \quad (24)$$

populates the eliminated state $|p\rangle$. Temporarily reintroducing $|p\rangle$ at jump times, followed by immediate jumps to the lower lying states by $\hat{L}_{\text{temp}}^{\gamma_p, j} = \sqrt{c_j\gamma_p}|j\rangle\langle p|$, allows accurate simulation of the decay processes. Our system is depicted in Fig. 3 and the parameters chosen for simulation are summarized in Table II.

The Monte Carlo wave functions on average yield the density matrix. This is true for any ensemble size, while the statistical errors on the estimate decrease with large n . The trace distance and the fidelity measures are not linear functions in the density matrix elements. Hence sampling their values with a finite wave function ensemble may provide a systematic error in addition to the statistic uncertainty of the method. In Ref. [24] a nonlinear master equation was analyzed and the systematic error was estimated to scale as $1/n$, thus becoming less important than the statistical error ($\sim 1/\sqrt{n}$) for large ensembles. Convergence of the AAWF method is illustrated in Fig. 4 where trace distance $T(\tilde{\chi}, \chi)$ and fidelity $F(\tilde{\chi}, \chi)$ are recorded for different Monte Carlo wave function ensemble sizes. For each ensemble size, we have made 50 simulations and at $n = 500$ sample-to-sample

TABLE II. Physical parameters for our simulations based on values discussed in Refs. [22,23].

Experimental parameter	Symbol	Value
Detuning	$\Delta/2\pi$	2.0 GHz
Red Rabi frequency	$\Omega_R/2\pi$	118 MHz
Blue Rabi frequency	$\Omega_B/2\pi$	39 MHz
Rydberg blockade	$\mathcal{B}/2\pi$	20 MHz
Decay rate ($ p\rangle$)	$\gamma_p/2\pi$	6.07 MHz
Decay rate ($ r\rangle$)	$\gamma_r/2\pi$	0.53 kHz
Dephasing rate ($ r\rangle$)	$\gamma_d/2\pi$	1.0/2.0 kHz

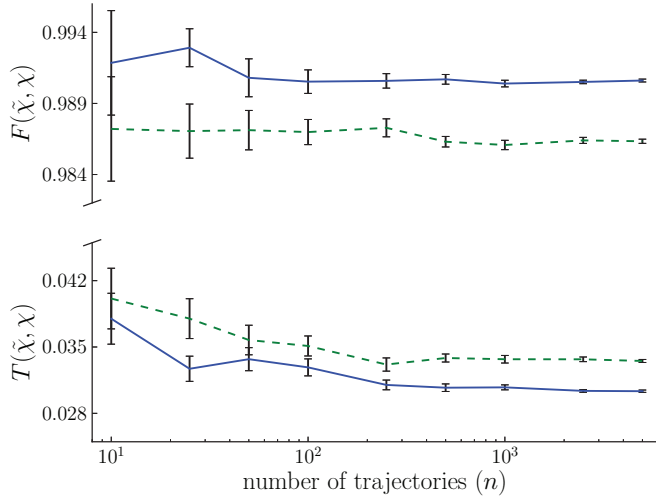


FIG. 4. (Color online) Convergence of the process fidelity and trace distance determined by the ancilla-assisted wave function characterization method. For selected values of n the mean value and standard deviation of the fidelity (top) and trace-distance (bottom) is obtained using 50 samples. Each sample involves a process matrix simulation with n trajectories. The solid lines represent calculations using the parameters in Table II with $\gamma_d/2\pi = 1.0$ kHz. The dashed lines are obtained with the higher dephasing rate $\gamma_d/2\pi = 2.0$ kHz.

variations are small enough to consider the output results satisfactorily converged.

In Figs. 5(a) and 5(b), we show the real and imaginary part of the difference between the process matrix elements obtained by our simulations and the ideal C-PHASE gate. Figure 5(c) shows the trace distance between the gates as function of the blue laser Rabi frequency for different values of the Rydberg blockade shift. The solid curves are based on our simulations with ensembles of $n = 500$ Monte Carlo wave functions, while the dashed curves are upper bound

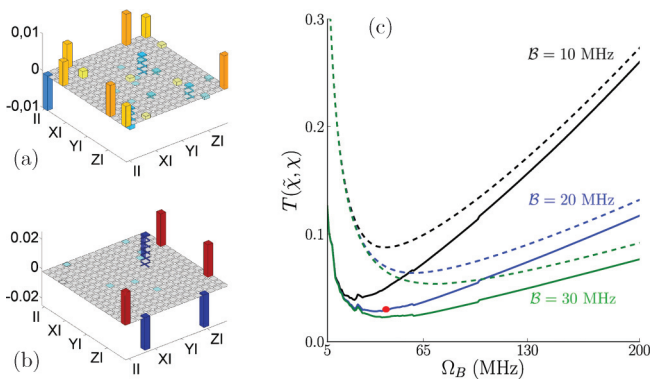


FIG. 5. (Color online) Simulating the χ matrix with AAWF. (a) Real and (b) imaginary part of the difference between the ideal and simulated process matrix for a C-PHASE gate [N.B. Sub-tick labels to the right of each $\mathcal{W}I$ read $\mathcal{W}X, \mathcal{W}Y, \mathcal{W}Z$, where $\mathcal{W} \in \{I, X, Y, Z\}$]. (c) Trace distance as a function of the blue laser Rabi frequency for three experimental realizations of blockade strength: full AAWF treatment (solid line) and “no-jump wave function” upper bound (dotted line). The (red) dot on the solid $B = 20$ MHz line indicates the parameters used in parts (a) and (b) of the figure. We use the parameters listed in Table II with $\gamma_d/2\pi = 1.0$ kHz.

calculations using a single no-jump trajectory for each set of parameters; cf. Sec. VI. The figure confirms that the upper bound indeed exceeds simulation results and, given its simplicity, provides a reasonable characterization of the errors. To understand the variation of the trace distance for small values of Ω_B we recall that the gate time $t_{\text{gate}} \propto 1/\Omega_{\text{eff}}$. As $\Omega_B \rightarrow 0$ the gate time lengthens, and errors due to intermediate state decay and dephasing increase. On the other hand, as $\Omega_{\text{eff}} \simeq \Omega_B \Omega_R / \Delta \rightarrow B$ from below, the gate errors increase due to population leakage into the $|rr\rangle$ state. We thus find an optimum value for Ω_B between these two regimes. Although certain to pose experimental challenges, the simulation also records advantages to gate quality by increasing B to 30 MHz.

VIII. DISCUSSION AND CONCLUSION

In conclusion we have presented a numerically efficient method to obtain the χ matrix for an arbitrary quantum process from a solution to the system’s master equation. Monte Carlo wave functions present an effective means to simulate the system density matrix and extend in a natural way to model ancilla-assisted process characterization. Parameterizing the outcomes of the simulated system under a fixed set of operations we presented a ζ vector representation of the Monte Carlo wave functions. Because the process matrix χ results as a simple product of ζ vector components the numerical effort to both simulate state evolution and represent the process adequately were significantly reduced. We also showed why this method is preferred over a straightforward retrieval of output density matrices from averaged wave function components. The Monte Carlo wave function method provides the further insight that, in the case of little dissipation, a single “no-jump” trajectory is enough to find an upper bound on trace distance between the ideal χ and the simulated one. Such upper bound estimates may be helpful in estimating optimal parameters for experiments. Furthermore, our analysis showed that the mathematical inversion problem occurring in standard process characterization can be solved in the much lower dimensional vector space. Although identified by our state vector formalism it may be applied to density matrices in usual process tomography.

Our method was demonstrated on the Rydberg-mediated two-qubit C-PHASE gate. In future work we plan to address larger quantum systems for which reliable error estimates are needed. Multibit gates and the application of consecutive gates together with realistic simulations of error correction codes constitute appealing applications of our numerically efficient method.

ACKNOWLEDGMENTS

The authors gratefully acknowledge discussions with Mark Saffman. This work was supported by the IARPA MQCO program through ARO contract W911NF-10-1-0347.

APPENDIX

Let $\{|j\rangle\} : j = 1, \dots, D^2$ be a linearly independent basis for the D^2 -dimensional vectors on the principal-ancilla space $P \otimes A$. The initial bipartite system-ancilla state vector $|\Psi\rangle\rangle = \sum_{r=1}^D |r\rangle \otimes |r\rangle$ evolves during the Monte Carlo simulation

of the process \mathcal{E} into a (stochastic) state vector that can be expanded in this basis:

$$|\Psi_{\mathcal{E}}\rangle = \sum_j \lambda_j |j\rangle. \quad (\text{A1})$$

Averaging the outer product of many of these states yields the outcome of the master equation evolution of the initial entangled density operator $\mathcal{O} = |\Psi\rangle\langle\Psi|$. Since $\mathcal{O} = \sum_{r,s=1}^D \mathcal{O}_{rs} \otimes \mathcal{O}_{rs}$ [Eq. (8)] we obtain

$$\begin{aligned} \overline{|\Psi_{\mathcal{E}}\rangle\langle\Psi_{\mathcal{E}}|} &= (\mathcal{E} \otimes \mathcal{I})(\mathcal{O}) = \sum_{rs} \mathcal{E}(\mathcal{O}_{rs}) \otimes \mathcal{O}_{rs} \\ &= \sum_{rs} \sum_{pq} \Lambda_{rs,pq} \mathcal{O}_{pq} \otimes \mathcal{O}_{rs}, \end{aligned} \quad (\text{A2})$$

where $\{\mathcal{O}_{pq} = |p\rangle\langle q| : p, q = 1, \dots, D\}$ is a linearly independent basis for the space of $D \times D$ linear operators.

In Eq. (14) we define

$$(E_m \otimes I)|\Psi\rangle = \sum_j \kappa_j^m |j\rangle, \quad (\text{A3})$$

and expansion of the outer product of two such states yields

$$\begin{aligned} (E_m \otimes I)|\Psi\rangle\langle\Psi|(E_n^\dagger \otimes I) &= E_m |r\rangle\langle s| E_n^\dagger \otimes |r\rangle\langle s| \\ &= \sum_{pq} \mathcal{K}_{rs,pq}^{mn} \mathcal{O}_{pq} \otimes \mathcal{O}_{rs}, \end{aligned} \quad (\text{A4})$$

where we have used the notation defined in Eq. (5).

In the text we define ζ as the solution to Eq. (15). By forming the outer product of

$$\sum_j \left(\sum_m \kappa_j^m \zeta_m \right) |j\rangle = \sum_j \lambda_j |j\rangle, \quad (\text{A5})$$

and averaging over many simulation outcomes, we obtain by Eqs. (A2) and (A4)

$$\sum_{mn} \mathcal{K}_{rs,pq}^{mn} \overline{\zeta_m \zeta_n^*} = \Lambda_{rs,pq} \quad (\text{A6})$$

for all r and s . Before Eq. (7) we identified the process matrix χ as the solution to the same equation $\sum_{mn} \mathcal{K}_{rs,pq}^{mn} \chi_{mn} = \Lambda_{rs,pq}$, and we have thus shown that χ is directly obtained from the ζ vectors, $\chi_{mn} = \overline{\zeta_m \zeta_n^*}$.

-
- [1] M. Nielsen and I. Chuang, *Quantum Computation and Quantum Information* (Cambridge University Press, Cambridge, 2010).
- [2] I. L. Chuang and M. A. Nielsen, *J. Mod. Opt.* **44**, 2455 (1997).
- [3] J. F. Poyatos, J. I. Cirac, and P. Zoller, *Phys. Rev. Lett.* **78**, 390 (1997).
- [4] D. W. Leung, *J. Math. Phys.* **44**, 528 (2003).
- [5] G. M. D'Ariano and P. Lo Presti, *Phys. Rev. Lett.* **86**, 4195 (2001).
- [6] J. B. Altepeter, D. Branning, E. Jeffrey, T. C. Wei, P. G. Kwiat, R. T. Thew, J. L. O'Brien, M. A. Nielsen, and A. G. White, *Phys. Rev. Lett.* **90**, 193601 (2003).
- [7] G. M. D'Ariano and P. Lo Presti, *Phys. Rev. Lett.* **91**, 047902 (2003).
- [8] M. Mohseni and D. A. Lidar, *Phys. Rev. Lett.* **97**, 170501 (2006).
- [9] M. Mohseni and D. A. Lidar, *Phys. Rev. A* **75**, 062331 (2007).
- [10] M. Mohseni, A. T. Rezakhani, and D. A. Lidar, *Phys. Rev. A* **77**, 032322 (2008).
- [11] X. L. Zhang, A. T. Gill, L. Isenhowe, T. G. Walker, and M. Saffman, *Phys. Rev. A* **85**, 042310 (2012).
- [12] Y. S. Weinstein, T. F. Havel, J. Emerson, N. Boulant, M. Saraceno, S. Lloyd, and D. G. Cory, *J. Chem. Phys.* **121**, 6117 (2004).
- [13] H. Carmichael, *An Open Systems Approach to Quantum Optics* (Springer, Berlin, 1993), Vol. 18.
- [14] J. Dalibard, Y. Castin, and K. Mølmer, *Phys. Rev. Lett.* **68**, 580 (1992).
- [15] K. Mølmer, Y. Castin, and J. Dalibard, *J. Opt. Soc. Am. B* **10**, 524 (1993).
- [16] R. Dum, P. Zoller, and H. Ritsch, *Phys. Rev. A* **45**, 4879 (1992).
- [17] C. Gardiner and P. Zoller, *Quantum Noise: A Handbook of Markovian and Non-Markovian Quantum Stochastic Methods with Applications to Quantum Optics* (Springer, Berlin, 2004), Vol. 56.
- [18] K. Kraus, A. Böhm, J. Dollard, and W. Wootters, *States, Effects, and Operations Fundamental Notions of Quantum Theory* (Springer-Verlag, Berlin, 1983), Vol. 190.
- [19] F. Bardou, J. P. Bouchaud, O. Emile, A. Aspect, and C. Cohen-Tannoudji, *Phys. Rev. Lett.* **72**, 203 (1994).
- [20] A. Gilchrist, N. K. Langford, and M. A. Nielsen, *Phys. Rev. A* **71**, 062310 (2005).
- [21] F. Reiter and A. S. Sørensen, *Phys. Rev. A* **85**, 032111 (2012).
- [22] T. A. Johnson, E. Urban, T. Henage, L. Isenhowe, D. D. Yavuz, T. G. Walker, and M. Saffman, *Phys. Rev. Lett.* **100**, 113003 (2008).
- [23] M. Saffman, X. Zhang, A. Gill, L. Isenhowe, and T. Walker, *J. Phys. Conf. Ser.* **264**, 012023 (2011).
- [24] Y. Castin and K. Mølmer, *Phys. Rev. A* **54**, 5275 (1996).